Mass-transport properties of electrosprayed Pt/C catalyst layers for polymer-electrolyte fuel cells.

Julio J. Conde[1], M. Antonia Folgado[1], P. Ferreira-Aparicio[1], Antonio M. Chaparro[1,*],

Anamika Chowdhury[2], Ahmet Kusoglu[2], David Cullen[3], Adam Z. Weber[2]

1) Energy Department, CIEMAT, Avda. Complutense 40. 28040 Madrid, Spain

2) Energy Conversion Group, Energy Technologies Area, Lawrence Berkeley National Laboratory, 1 Cyclotron Road, Berkeley, California 94720, USA

3) Center for Nanophase Materials Sciences, Oak Ridge National Laboratory, Oak Ridge, Tennessee 37831, USA

- Declarations of interest: none

*Corresponding author:

Antonio M. Chaparro

Energy Department, CIEMAT, Avda. Complutense 40. 28040 Madrid, Spain

antonio.mchaparro@ciemat.es

Telephone: +34 913460897

Fax: +34 913466269

ABSTRACT

Mass-transport properties of electrosprayed catalyst-layers based on Pt/C and ionomer (Nafion) are studied with hydrogen limiting-current technique, water-vapor-uptake, scanning transmission microscopy (STEM), single-cell testing, and impedance spectroscopy. The hydrogen limiting-current technique provides the transport resistance of the layers (R_{CL}^{mt}), which shows to be lower in electrosprayed layers compared with conventional layers, especially at very low platinum loadings (0.025 $mg_{Pt} \cdot cm^{-2}$) and low cell temperature, denoting superior mass-transport properties. Images of the distribution of Pt, F, and C elements reveal the ionomer preferentially interacting with the Pt nanoparticles. Water-vapor-uptake experiments show larger vapor absorption for electrosprayed than conventional catalyst layers. Such large water-vapor uptake capability is combined with superhydrophobicity, ie. very low interaction with water in liquid phase (wettability). Both apparently contradictory properties result from a particular configuration of the amphiphilic ionomer in the electrosprayed layers, and provide ideal conditions for high mass transport and ionic conductivity in a catalyst layer. Electrosprayed layers as cathode catalyst layers show peak response at a loading of 0.17 $mg_{Pt} \cdot cm^{-2}$ (18 µm layer thickness when using Pt/C 20 wt% catalyst) where they provide minimal mass-transport and polarization resistances.

Keywords: PEMFC, catalyst layer, electrospray, mass transport, water uptake, thin porous film

1. Introduction

Mass transport in the catalyst layer of proton-exchange-membrane fuel cells (PEMFCs) has a significant impact on fuel-cell performance and durability. Within the catalyst layer, mass transport of reactants (O_2, H_2) and product (water) take place near the catalyst sites, resulting in local transport resistances that impact polarization behavior. In addition, the transport of liquid water in the catalyst layer controls the membrane and electrodes humidification states that determine key parameters for fuel cell performance, like the internal resistance and the catalyst activity. The catalyst layer must allow for facile transport of gas and liquid water, high proton conductivity, and easy accessibility of catalytic sites, keeping at the same time optimal membrane humidification [1,2,3].

A promising catalyst-layer fabrication technique is electrospray deposition, which enables one to produce catalyst layers with particular morphology, transport properties, and wettability [4,5,6,7,8,9]. The electrospray deposition uses a suspension of catalyst particles (Pt/C) and nanometer ionomer aggregates (Nafion) which is ejected through a nozzle under the influence of a strong electric field. By these means, the suspension is transferred to an aerosol of charged particles where the solvent evaporates, so they are dry deposited and discharged on the substrate under electrostatic interactions. The substrate can be the gas-diffusion layer (GDL) or the proton-exchange membrane [10]. Dendritic morphologies and a specific interaction between the catalyst and the ionomer have been observed in the electrosprayed films, however the exact nature is yet unknown. Under appropriate deposition conditions, the layers present a superhydrophobic surface, ie. a surface characterized by water drop contact angles $\theta > 150^o$. Such superhydrophobicity is a result of the Nafion distribution, catalyst agglomerates arrangement, and dendritic morphologies that cover the surface of the agglomerates. Superhydrophobicity extends

internally into the surface of the macropores that are formed during the electrospray process by the sequential incorporation of ionomer and catalyst particles [11]. The result is a *superhydrophobic porous layer* with particular properties for liquid-water transport and interaction. One principal property is that the absorption of liquid water into the macropores requires larger capillary pressures, ie. pressure difference between the liquid and the gas phases (p_c=p_L-p_G), than for less hydrophobic layers; consequently, they operate under lower saturation (ie. less liquid water occupation in the pores) in a PEMFC, where the capillary pressure is imposed by the working conditions. In addition, liquid water tends to stay as isolated drops, instead of continuous domains filling the pores space in more hydrophilic catalyst layers [12], and, preferentially, inside the larger than the smaller macropores of identical hydrophobicity [13], formed during the electrospray deposition. Such characteristics have a large impact on their behavior as catalyst-layer because they affect water and oxygen transport [14,15]. As a result, PEMFC with cathodic electrosprayed layers show improved performance with respect to conventional layers, especially under high current densities, leading to peak power densities 20% larger [10,11]. The electrosprayed layers favor highly homogeneous current distribution through the electrode and enhance the liquid-water back-transport process, ie. water flux from the cathode through the membrane towards the anode, keeping optimal humidification conditions in the whole cell during operation. As a consequence they increase cell durability under cyclic start-up/shut-down operation [16] or under dry gas feeds [17].

The study of mass-transport properties of superhydrophobic electrosprayed catalyst layers may help better understand their behavior as catalyst layers, and in particular the impact of the superhydrophobicity and related ionomer properties. In addition, electrosprayed layers may be an option in the drive for low catalyst loadings in PEMFC electrodes, and thus lower material costs, which appears limited by the increased gas-transport limitations at the reaction site ('local mass

transport resistance') [18,19,20,21]. The mass-transport resistance can be measured using limiting-current techniques with either hydrogen or oxygen [22,23,24,25,26,27]. In the hydrogen limiting-current technique, the GDL and catalyst-layer resistances (R_{GDL}^{mt} and R_{CL}^{mt}, respectively) can be distinguished without the influence of water production or sluggish kinetics, and the possibility of using D_2 and H_2 allows one to separate out the nature of the resistance [19,22].

Mass transport resistance of the catalyst layer has been analyzed with a continuum, one-dimensional model that assumes gas-filled pores [28]. According to this model, R_{CL}^{mt} is composed of two contributions: the 'through plane resistance', due to transport through the macro/meso porous catalyst-layer structure in the direction perpendicular to the catalyst-layer plane; and the 'local resistance' (R_{Local}) that accounts for transport limitations very close to the reaction site. The following mathematical expression has been obtained for R_{CL}^{mt} with the two referred terms [27,28,29]:

$$R_{CL}^{mt} = \frac{L}{3D_{CL}} + \frac{R_{Local}}{\eta\gamma r_f} \quad (1)$$

Where L is the catalyst-layer thickness, D_{CL} is the effective reactant gas diffusion coefficient in the pores of the inter-agglomerates space of the catalyst layer, ie. corrected for porosity (ϕ) and tortuosity (τ) ($D_{CL}=\phi D/\tau$), r_f the catalyst roughness factor, γ (~0.365 for 20 wt% Pt/C particles) is the fraction of catalyst (Pt) surface in the external surface of agglomerates (because it is the only active under mass transport limitation) related to total catalyst surface, and η (~2-5 - 2.9 for ionomer thickness 5 - 10 nm) is a focusing factor that accounts for the discreteness of Pt surface on the agglomerates. Eq.1 is able to explain the observed increase in R_{CL}^{mt} at very low loading, which is implicit in the second term of the right.

In this work, R_{CL}^{mt} of electrosprayed catalyst layers is measured by the hydrogen limiting-current technique to study their mass-transport behavior, and complemented with water-vapor uptake, microscopy, single cell results, and impedance analysis. Transport characteristics of electrosprayed films are compared with those of conventional airbrushed films. The results provide a more complete picture of the behavior of electrosprayed layer and their high performance and durability in PEMFC.

2. Experimental

Electrospray deposition of Pt/C+ionomer (Nafion) on membrane was carried out as described elsewhere [10]. Suspensions (1 wt% solids concentration) were prepared by mixing Pt/C commercial catalyst powder (E-TEK, 20 wt% on Vulcan XC-72R) with Nafion^R solution (Aldrich, 5wt%) in isopropanol (Panreac) solvent, and stirred in an ultrasonic bath during about 2 hours prior to electrospray deposition. The suspension is put in a vessel under a small N_2 overpressure (0.1-0.5 bar_g), and conducted to a metallic ejector through a silica capillary. A dc voltage (4 - 9 kV) is imposed between the ejector (positive pole) and the substrate (negative pole) by means of a high voltage source (Bertran, Model 205B-10R). The substrate was Nafion NRE212 (Ion Power Inc.) with 15.2cm^2 active area, thermostated at 50^{o}C, and placed on a computer controlled x-y stage. Deposition was carried out in successive sweeps, at a rate of 8 $\mu l \cdot min^{-1}$, with the suspension under ultrasonic agitation and thermostated at 22^{o}C. Airbushed layers were prepared on Nafion NRE212 from suspensions of Pt/C and Nafion, using an airbrush (Vega Systems), in successive sweeps using the same x-y stage and ink conditioning as for the electrospray deposition.

Single cells were mounted with the electrosprayed catalyst layer and a commercial gas diffusion layer (GDL) (ELAT GDL LT1200W) in the cathode side. In the anode side, a commercial electrode was used (ELAT GDE LT250EWALTSI, BASF, 0.25 $mgPt \cdot cm^{-2}$). Anodic and cathodic flow field plates

were gold plated stainless steel (Grade 310S, 2mm thickness) with double serpentine flow channels (1mm x 1mm section). Gas tightness was accomplished with silicone gaskets. Current collectors were gold plated brass plates, and end plates were stainless steel plates (8 mm thickness) clamping the structure with 8 screws tightened to a controlled torque (3 N·m).

Single-cell testing was carried out using a home-made test bench, under controlled back pressure and temperature of the cell, gases feeding through mass flow controllers, heated pipes, and thermostated humidifiers. Cell current was drawn with an electronic load (HP 6060B), while monitoring cell voltage and internal resistance at 1 kHz (HP Agilent 4338A milliohmmeter). Testing followed a protocol consisting of cell start-up and heating to 80ºC during first 12 hours, under a 60 $mA \cdot cm^{-2}$ current demand; after a steady-state is attained (normally after 24 h), polarization curves and impedance spectroscopy measurements are carried out. Polarization curves were taken at 80ºC, 1 bar_g, under H_2 (Air Liquide, 99.999%) and O_2 (Air Liquide, 99.995%) flow at constant stoichiometric factor (1.5 and 3, respectively), and 100% inlet relative humidity. Cathode electroactive area measurements were carried out by the hydrogen underpotential deposition method, at 30ºC, and 25 $mV \cdot s^{-1}$, feeding the single cell with 100% RH, H_2 in anode and N_2 in cathode, and 40 $ml \cdot min^{-1}$ flow rate. Impedance spectroscopy was taken in potentiostatic mode superposing 10mV RMS sinusoidal voltage (Autolab 30N with 10A current booster), from 20 kHz to 0.1 Hz. The impedance spectra were analyzed using commercial software (Nova, Autolab).

For mass transport resistance measurements on electrosprayed and airbrushed catalyst layers deposited on Nafion NRE212 membranes, the hydrogen limiting-current technique was used, as described elsewhere [18,19,22,23]. The catalyst coated membranes were put in contact with a Sigracet 24BC (w/ MPL & 5%PTFE) GDL as testing electrode, and an ELAT ETEK GDE as counter electrode. Exposed electrode area was 0.713 cm^2. The counter electrode was fed with 2%

hydrogen diluted in argon, while the testing electrode was fed with 1000 ppm H_2 (or D_2) diluted in argon with constant flow set at 200 and 500 cm^3 min^{-1} respectively, and atmospheric pressure. The MEAs were first conditioned with 25 cyclic voltammetries, from 0.08 to 0.95V at 50 mV s^{-1}, followed by another 25 cleaning voltammetries at 100 mV s^{-1} with pure argon in the working electrode. Before switching gases, a potential hold is applied to calculate the crossover current values. Afterwards, limiting current (i_{lim}) with hydrogen and deuterium is measured recording the current at 0.3 V after a steady state is reached. Catalyst-layer mass transport resistance (R_{CL}^{mt}) was obtained from the total resistance measured (R_{Total}^{mt}):

$$R_{total}^{mt} = R_{CL}^{mt} + R_{GDL}^{mt} + R_{foil}^{mt} \quad (2)$$

Where:

$$R_{total}^{mt} = \frac{nFc_{Avg}^{Feed}}{i_{lim}} \quad (3)$$

Where n(=2) is the number of electrons exchanged during hydrogen oxidation ($H_2 \rightarrow 2H^+ + 2e^-$), F(=96485 C·mol^{-1}) the Faraday constant, c_{Avg}^{Feed} is the averaged reactant feed concentration in the flow channels of the measuring cell (1000 ppm), and i_{lim} is the measured limiting-current density. The mass-transport resistive components of the cell, ie. the gas-diffusion layer R_{GDL}^{mt} and the copper foil aperture used as current collector, R_{foil}^{mt}, are typically < 1 s·m^{-1}, well below those of R_{CL}^{mt}, so the measured mass-transport resistance can be almost entirely attributed to the catalyst layer [29]. Each experiment was repeated at least three times, and the error determined for the mass transport resistances is 10%, including measurements error and representative sample to sample variability.

Scanning transmission electron microscopy (STEM) and electron dispersive X-ray spectroscopy (EDS) characterization were performed for cross sectional analysis of morphology and composition

of the films [30,31]. The measurements were carried out using an FEI Talos F200X (Oregon, USA) operated at 200kV, which is optimized for high X-ray collection efficiency by the integration of four symmetrically arranged 30 mm^2 active-area silicon drift detectors within the microscope column, resulting in a solid angle of 0.9 sr. Count-based fluorine elemental maps were acquired and were used to examine the ionomer distribution in the CLs relative to Pt . Cross-section MEAs were embedded in epoxy and cured at 60^oC. The resulting blocks are trimmed and then sectioned into 75 nm thick cross sections by diamond knife ultramicrotomy.

The water uptake of the samples as a function of relative humidity (RH) and temperature was characterized using a dynamic-vapor-sorption (DVS) analyzer (Surface Measurement Systems, UK). With this aim, the catalyst layers were deposited by electrosprayed and airbrush deposition on porous Teflon substrates (Whatman® TE-35 PTFE membrane filters, 0.2 µm pore size (Sigma Aldrich), with 0.25 $mg \cdot cm^{-2}$ platinum loading and different Nafion concentrations. Porosity of the PTFE substrate ensures that the samples have full access to the flowing humid gas, and, at the same time, provides some ionic conduction necessary for electrospray deposition on non-conducting substrates [10]. A sample was also prepared with carbon black (Vulcan XC-72R) and 15 wt% Nafion concentration. The samples were first equilibrated at 0% RH at 25°C for two hours to achieve the dry state, after which the initial (dry) weight of the sample, ($M_{TFE} + M_0$) was set. The sample was hydrated using humidified nitrogen feed to increase the RH in steps of 10% up to 90% and then to 95% or 98%, then dehumidified back to 90% and to 0% in the same manner. The membrane was equilibrated at each RH step for at least 1 hour or until the change in the weight $\Delta M/(M_{PTFE} + M_0)$ was less than 0.005 %/min. In some cases, samples reached steady-state in as little as 10 minutes. The weight of water absorbed by the sample, M_w, is determined from the measured weight of humidified sample, M_{humid}, and its initial weight, i.e.:

$$M_W = M_{humid} - (M_{PTFE} + M_0) \quad (4)$$

Since M_W is enterely absorbed in the CL, the water fraction absorbed related to its weight is:

$$\Delta M = \frac{M_W - M_0}{M_0} \times 100. \quad (5)$$

Where the M_0 values were determined for each sample. If we assume that all the water absorbed is interacting with the ionomer sulfonic groups, then the ionomer water content, λ, which represents the number of water molecules per sulfonic-acid group of ionomer, can be calculated from:

$$\lambda = \frac{M_W/\bar{M}_W}{M_i^{dry}/EW}, \quad (6)$$

where M_i^{dry} is the dry weight of the ionomer in CL sample, EW [g/mol] is the equivalent weight of the ionomer (1100 g/mol for all samples used in this study) and $\overline{M_W}$ is the molar weight of water (18 g·mol^{-1}). The dry weight of the ionomer is the weight fraction of ionomer, f_i, put in the catalyst layer:

$$M_i^{dry} = f_i M_0 \, . \quad (7)$$

3. Results

3.1 Catalyst layer mass-transport resistance (R_{CL}^{mt})

The mass-transport resistance of the catalyst layers was measured for different ionomer and Pt/C concentrations, and at different gas humidities and cell temperatures. Measurements were carried out using H_2 and D_2 to probe molecular-weight specific effects on the mass transport. The results are shown in Fig. 1, together with the ratio of transport resistances with both gases, $R^{D2}{}_{CL}/R^{H2}{}_{CL}$.

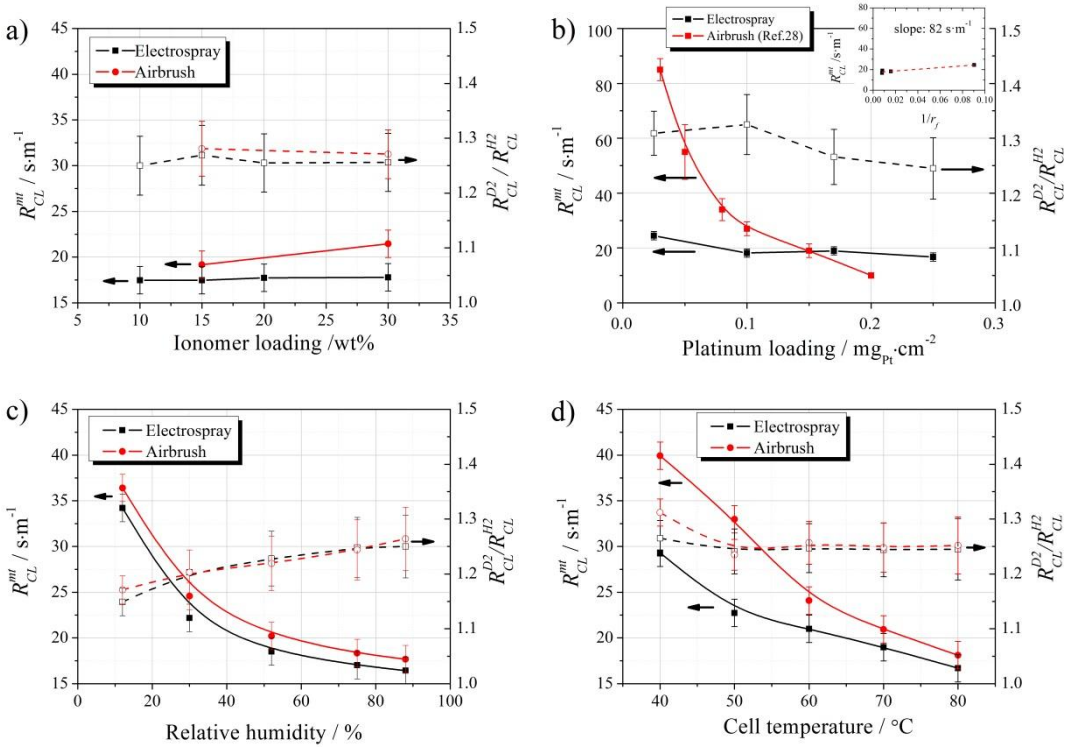

Fig.1. Mass-transport resistance (R^{mt}_{CL}), and molecular-weight specific resistances ratio (R^{D2}_{CL}/R^{H2}_{CL}, dashed line), as a function of ionomer concentration (a), Pt loading (constant Pt/C) (b), gas relative humidity (c), and cell temperature (d), for electrosprayed (black) and airbrushed (red) catalyst layers. In a) and b), measuring conditions are 80°C and 80% RH. In b), electrosprayed films contain 15 wt% ionomer loading, whereas the data of airbrushed film are taken from ref.28, and correspond to films prepared with 37 wt% ionomer loading. In c) and d), the catalyst layers have 0.25 mg·cm^{-2} Pt loading, and 15 wt% ionomer concentration. The inset in (b) shows the $R_{CL}{}^{mt}$ vs. $1/r_f$ plot (see the text).

The electrosprayed films are characterized by lower $R_{CL}{}^{mt}$, compared with airbrushed films, for all compositions and measurement conditions tested. Fig.1a shows that the ionomer concentration has minor influence on $R_{CL}{}^{mt}$ of the electrosprayed layers, whereas for airbrushed layers $R_{CL}{}^{mt}$ increases significantly with ionomer loading. Such result indicates that the electrospray deposition

accommodates better larger amounts of the ionomer, having a minor impact on the transport properties of the films. The same conclusion was attained from porosity measurements in a previous work [5], and reflects an optimized distribution of the ionomer phase around the catalyst particles as determined herein. The effect of platinum loading on R_{CL}^{mt} of electrosprayed layers is shown in Fig.1b. A slight increase occurs at the lowest loadings, which is less severe than the observed in conventional layers [18,20,22,28]. In [22], an increase from 22.5 $m \cdot s^{-1}$ to 52.3 $m \cdot s^{-1}$ when decreasing loading from 0.24 $mg.cm^{-2}$ to 0.028 $mg \cdot cm^{-2}$, using 40 wt% ionomer loading, was registered for a conventional catalyst layer. The R_{CL}^{mt} data from [28] have been included in Fig.1b for comparison. It shows that electrosprayed films are able to better ameliorate the inherent mass-transport losses at low Pt loadings. Such losses are mostly attributed to the local mass-transport resistance, ie. transport losses very close to the reaction site, represented by the term $R_{Local}/\eta\gamma$ in Eq. 1. An estimation of this term can be obtained from the slope of the linear relation R_{CL}^{mt} vs. $1/r_f$, as shown in the inset of Fig.1b. The value obtained, 82 $s \cdot m^{-1}$, is 20 times lower than that measured for a conventional catalyst layer prepared with the same catalyst type (20 wt%) [28], showing improved local mass transport in electrosprayed catalyst layers.

Fig.1 also shows the ratio of resistances using deuterium and hydrogen ($R^{D2}{}_{CL}/R^{H2}{}_{CL}$) as gas probes. This ratio reflects the character of the transport process, approaching $R^{D2}{}_{CL}/R^{H2}{}_{CL}$ = 1.4 for molecular diffusive processes and decreasing when other transport processes, less dependent or independent of the molecular weight, are limiting [22,27]. The principal molecular diffusive processes in the catalyst layer occur for the transport of gases in the pores structure of the catalyst layer and inside the ionomer phase, whereas other relevant processes are the interfacial transport between the different phases present in the pores of the layer (gas, liquid, ionomer, catalyst surface), and surface diffusion over the catalyst particle. Hydrogen transport processes appear to be similar in electrosprayed and conventional catalyst layers in terms of dominant

resistance losses being about equal between molecular-weight independent and dependent transport mechanisms. Modeling described in [28,29] allows calculating the molecular-weight-dependent transport contribution to the transport resistance (see Supplementary Material, Fig.S1), which shows an increasing limitation by diffusive processes at low loadings due to local diffusion within the ionomer film. On the other hand, non-diffusive transport phenomena increase limitation at high catalyst loadings, ascribed to transport processes through ionomer/pore and ionomer/Pt interfaces [28].

Gas humidification has almost the same effect on both film types (Fig. 1c), showing a decay with humidity that is consistent with transport through the ionomer film being the most determining transport process. The decreasing $R^{D2}{}_{CL}/R^{H2}{}_{CL}$ at low humidities reflects more difficulties with interfacial transport. However, limiting-current measurements at low RH could also be affected by drying of the cell membrane. Cell temperature exhibits, on the other hand, different effect on transport properties for the two catalyst layers, as shown in Fig.1d; larger slope of the airbrushed film reflects larger thermal activation of transport than in electrosprayed films, especially at low temperature (< 50^{o}C). Similar $R^{D2}{}_{CL}/R^{H2}{}_{CL}$ in both layer types demonstrates that the controlling transport processes must be qualitatively similar in both catalyst-layer types, with some more differences at the lowest temperature (40^{o}C). The larger thermal activation of the airbrushed layer may be a consequence of its lower water-vapor-uptake capability (see below), which determines hydrogen transport within the ionomer film.

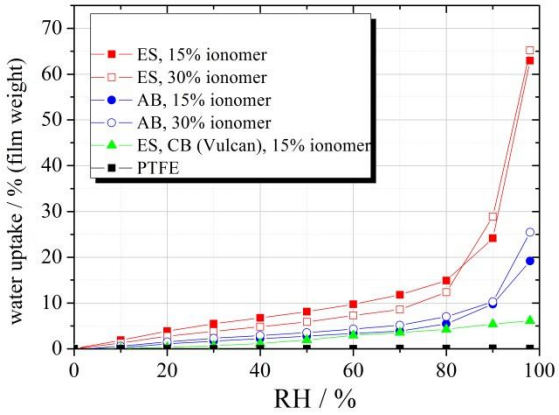

Fig. 2. Water-vapor uptake desorption curves (see Supplementary Material, Fig. S2, for absorption curves and results of λ calculation), as a function of relative humidity, for catalyst layers deposited by electrospray and airbrushing. Results for the PTFE substrate are also included.

Water-vapor uptake measurements on catalyst layers prepared by electrospray and airbrushing are shown in Fig. 2. In these experiments, water vapor enters the macropores structure of the CL leading to a mass increase upon absorption/adsorption into the layer [32]. We notice in Fig.2a that the electrospray catalyst layer is characterized by larger water-vapor-uptake capacity than the airbrushed layers in the whole range of relative humidities. Such a result may explain partially their lower R_{CL}^{mt} due to better ionomer hydration (Fig.1c), and the good behavior that they show in fuel-cell operation under low humidification conditions [17]. Assuming that all water vapor absorbs into the ionomer, the water content λ can be calculated from Eq. 6; the result and comments are included in the Supplementary Information together with the absorption curves (Fig. S2). The data in Fig.2 also confirm that Pt plays a critical role in orientating the ionomer chains or perhaps concentrating them (see STEM data below), thereby resulting a much lower water uptake for only C containing layers, which is consistent with prior studies [32]. The time dependent water-uptake fraction, taken during the measurements in Fig.2, show higher rate for

water absorption in the electrosprayed film than in the airbrushed film, especially at low ionomer loading, which is a clear indication of the favored conditions for water-vapor interaction leading to larger water-vapor uptake capability (see Supplementary Information, Fig.S3).

It must be noted that the enhanced water-vapor uptake of the electrosprayed layers is accompanied by very low wettability and superhydrophobic character [11,16,**¡Error! Marcador no definido.**33,34]. Such apparently opposite properties must be a consequence of the catalyst layer and ionomer phase resulting from the electrospray deposition, with macropores walls containing dendritic structures that decrease the adhesion of liquid water, combined with the ionomer closely interacting with the platinum surface with enhanced reactivity with water vapor molecules (see Discussion). They also explain the capability for fast water transport while retaining high ionic conductivity, which is most appropriate for a catalyst layer in a PEMFC.

3.2 Cross sectional morphology under STEM

Information about morphology and components distribution in electrosprayed catalyst layers can be obtained from cross sectional STEM images. Fig. 3 shows images of a catalyst layer with a Pt load of 0.025 $mg \cdot cm^{-2}$ and an ionomer loading of 15 wt.% (respect to the total layer weight), deposited on Nafion NR212.

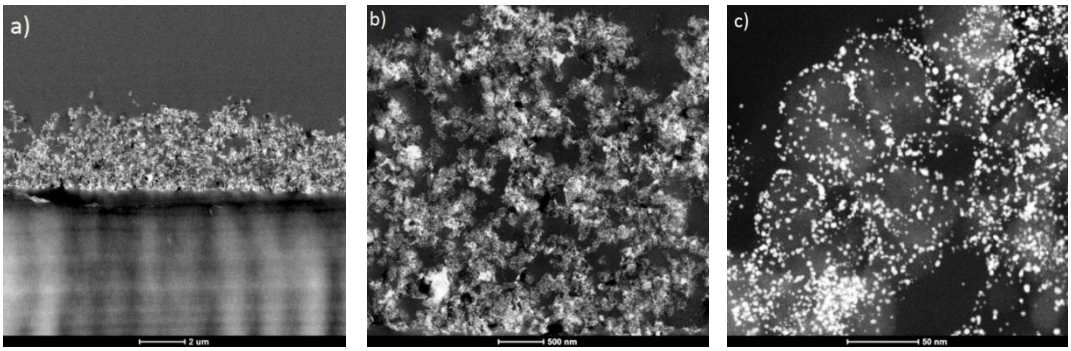

Fig.3. STEM images in cross section of an electrosprayed Pt/C + ionomer layer (0.025 mg·cm^{-2}, 15 wt% ionomer), at three different magnifications.

At lower magnification (Fig.3a) the layer shows irregular thickness, 3 to 4 µm, with large macropores (> 50 nm). At higher magnification (Fig.3b,c), the Pt catalyst nanoparticles appear evenly distributed showing no alteration at this level by the electrospray process [4].

The distribution of elements Pt, F, and C in the catalyst layer is shown in Fig.4. The STEM image shows Pt and carbon black phases (Fig.4a) that closely follow the contrasts of the Pt image (Fig. 4b) and the C image (Fig. 4c), respectively, as expected. Most significant in Fig.4 is the similarity between the distribution of Pt and F (cf Figs. 4b and c) in most areas (see the area inside the circle for example), that reflects a preferential interaction of the Nafion ionomer with Pt nanoparticles, and less with C support. Previous evidences of a specific interaction of the ionomer with Pt in electrosprayed films were obtained from thermogravimetric analysis [4]. STEM images of layers prepared with a common spray technique show, on the other hand, the ionomer covering uniformly all the surface of the particles [35].

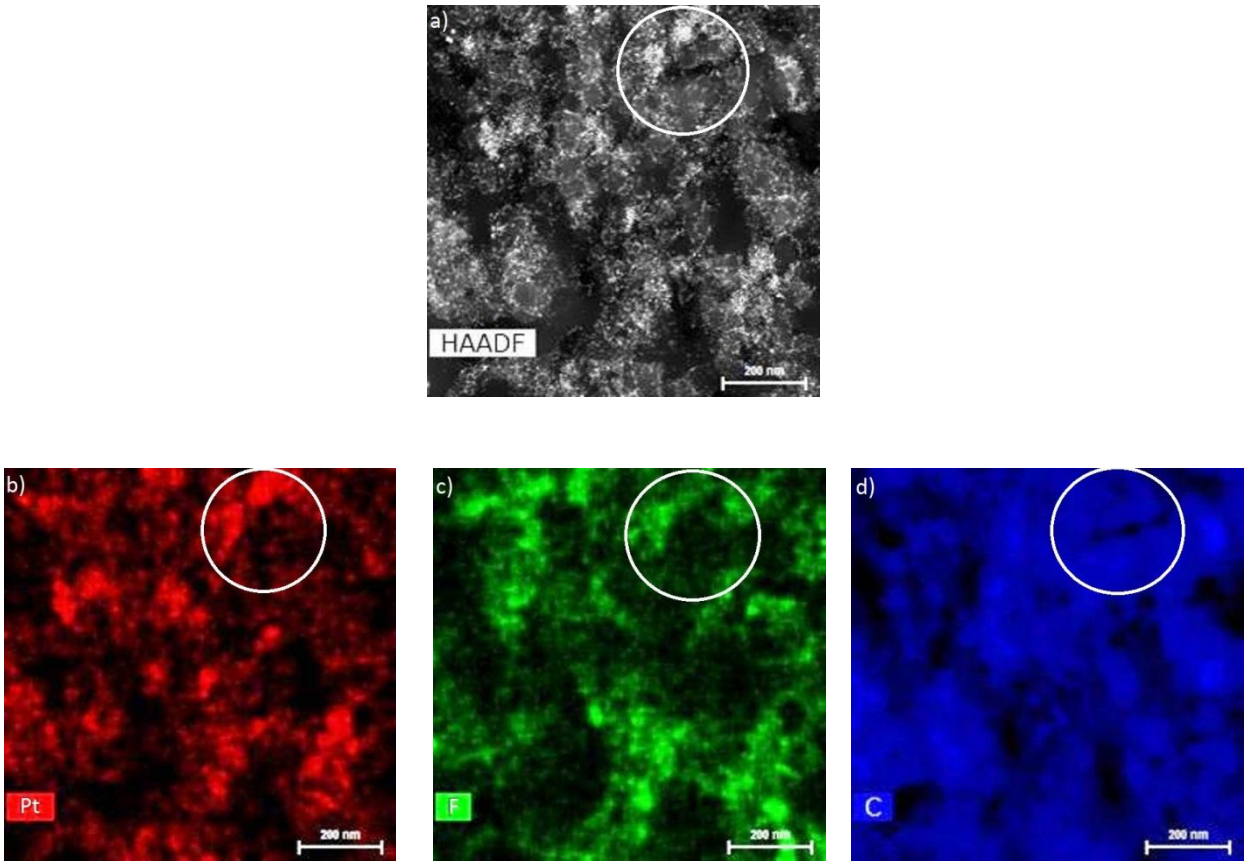

Fig.4. High-angle annular dark-field STEM image (a), and images of the distribution of Pt (b), F (c), and C (d). Circle for visual guide.

3.3 Single-cell testing

Single cells were mounted with electrosprayed catalyst layers in the cathodic electrode. Polarization curves and power density are shown in Fig.5, for four layers with different catalyst loadings.

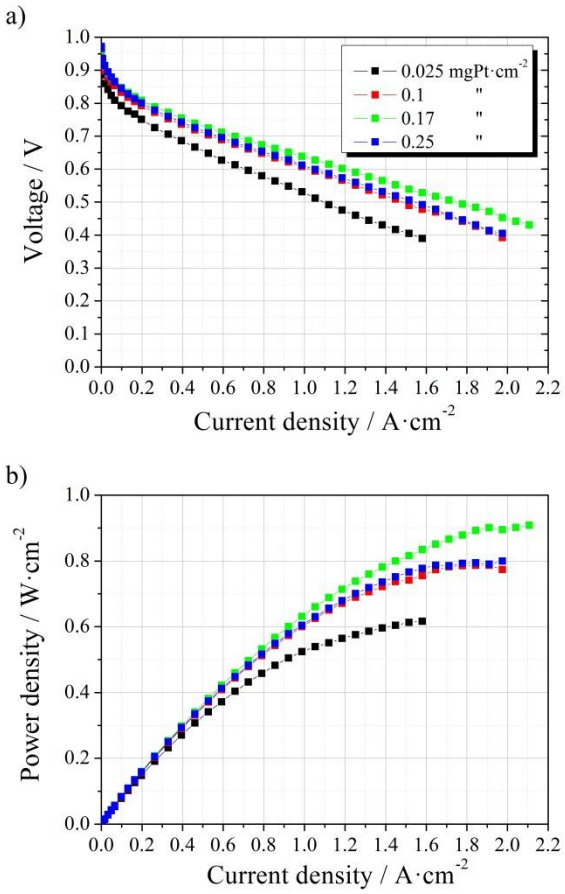

Fig.5. a) Polarization curves of single PEMFCs with electrosprayed catalyst layers of variable Pt loading in the cathode. b) Power density curves. Cells were tested at 80 ºC, 1 bar_g, and 100% RH conditions, using H_2/O_2 (1.5/3.0 stoichiometry) in anode/cathode. Polarization curves at 0% RH are shown in Supplementary Material, Fig.S5.

An optimal cell response is attained at a cathode loading of 0.17 $mg_{Pt}\cdot cm^{-2}$ in accordance with previous results [36]. The curves were analyzed using a simple 0-D equation:

$$V = E' - b \cdot log\frac{j}{r_f \cdot j_0} - j \cdot R_i^{dc} \quad (8)$$

Where V is the cell voltage, E' is the thermodynamic potential, b is the Tafel slope, j the current density, j_o the exchange current density per unit platinum area ($j_o = 8.5\cdot10^{-9}$ $A\cdot cm^{-2}_{Pt}$, [37]), r_f

($cm^2_{Pt}·cm^{-2}$) the roughness factor, and R_i^{dc} the dc internal resistance. The roughness factor was obtained from the measured electrochemical area ($r_f = L_{Pt} A_{Pt}$, where L_{Pt} is the platinum loading). Both, r_f and A_{Pt}, are plotted in Fig.6a as a function of platinum loading.

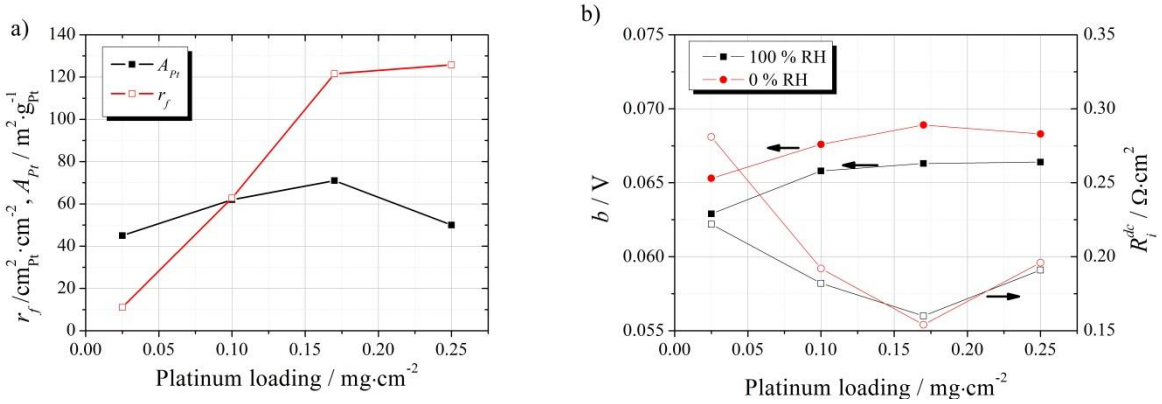

Fig. 6.- a) Roughness factor (r_f) and mass specific electrochemical area (A_{Pt}) of the electrosprayed catalyst layers of Fig.5 as a function of Pt loading. b) Tafel slope (b) and dc internal resistance (R_i^{dc}) at 100% RH and 0% RH, obtained from the least square fitting of polarization curves in Fig.5 to Eq.8.

A peak in the mass-specific Pt area is encountered at 0.17 $mg_{Pt}·cm^{-2}$, which reflects the conditions for the maximum accessibility of the platinum surface to reactants, which agrees with the maximum response in the polarization curves of Fig.5. A plateau in r_f and decrease in A_{Pt} at larger loadings (Fig.6a) is consistent with additional Pt being less accessible, although mass-transport is not worsen, as shown by the leveling of R_{CL}^{mt} at higher loadings in Fig.1b.

Results of the least-square-fitting analysis of polarization curves to Eq.8 are in Fig. 6b, where b and R_i^{dc} are plotted as a function of platinum loading, at 0% RH and 100% RH (Polarization curves at 0% RH are in Supplemenray Material, Fig. S5). For the fitting only points below 0.8 $A·cm^{-2}$ were considered to assure full catalyst layer limitation conditions (charge transfer and mass transport)

and without any other external mass transport limitation, as implicit in Eq.8 where the mass transport limitation term has been drop. According to the simple model used, parameter *b* gathers polarization losses in the catalyst layer, either due to kinetics, ohmic, or mass transport. The increase in *b* with catalyst loading must be attributed to ohmic losses occurring by the increasing thickness of the catalyst layer (thicknesses are provided in Supplementary Material, Fig.S4). The increase in Tafel slope with thickness of the catalyst layer, keeping constant the Pt loading, was encountered by M. Lee et al. in spray-coated membranes with variable Pt/C ratio [38], and T. Suzuki et al. [39] in coated membranes prepared with a doctor blade technique and blending Pt/C particles with stand-alone carbon black. The larger *b* registered at 0% RH than at 100% RH in Fig.6b could indicate either a decrease in catalyst performance, since liquid water in the catalyst layer favors the electrocatalysis of the oxygen reduction reaction [11,40], and/or additional mass transport losses at low RH and shifting of the reaction distribution next to the membrane. Most determining for fuel cell response, however, appears to be the evolution of R_i^{dc} in Fig. 6b. As a difference from the results of Tafel slopes, internal resistance shows almost no differences between 0% and 100% RH (except at the lowest loading), which is due to the electrosprayed catalyst layer keeping similar fuel cell performance under low humidity [17] (see also Fig.S5 in Supplementary Material). The minimum R_i^{dc} at 0.17 $mg_{Pt}{\cdot}cm^{-2}$ correlates with the maxima in A_{Pt} (Fig.6a) and cell performance (Fig.5). At this loading, conditions are optimal for the transport of gases, ionic conduction, and for Pt catalyst utilization in the electrosprayed cathodic catalyst layer, which are a consequence of its high water-vapor uptake capability and superhydrophobic character. More insight into the transport properties of the electrosprayed layers can be obtained from the impedance spectroscopy analysis.

3.4 Electrochemical impedance spectroscopy

Impedance spectroscopy was carried out on the cells with electrosprayed cathode catalyst layer. Nyquist plots exhibit one unique semicircle response at cell voltages between 0.8 and 0.6V (see Supplementary Material, Fig.S6), that is entirely ascribed to the catalyst layer impedance [41]. A second semicircle at low frequencies, reflecting transport losses in other parts of the cell, like the gas diffusion layers or the flow fields, is not observed at these cell voltages and operating conditions. The results of the analysis are shown in Fig.7, using the electrical circuit in the inset, where the series resistance element (R_s) accounts for the fast ohmic losses due to ionic conduction in the membrane and electronic conduction in the electrodes and contacts, R_{CL} accounts for transport and charge transfer losses in the cathodic catalyst layer, and the constant phase element (Y_{CL}, n) is related with the pseudo-capacitive character of this same layer [42].

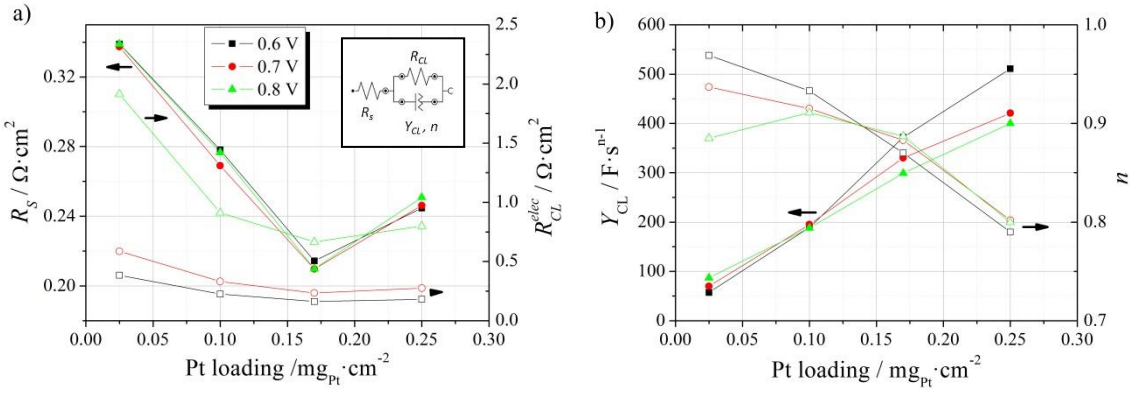

Fig.7. a) Series resistance (R_s, full symbols) and catalyst layer resistance (R_{CL}, open symbols) as a function of Pt loading in the electrosprayed catalyst layer, at three cell voltages. b) Constant phase element parameters, Y_{CL} (full symbols) an n (open symbols), as a function of catalyst loading, at three cell voltages. Inset in a) shows the electric circuit used for the impedance analysis. Cell conditions as in Fig. 5.

Cell series (R_s) and catalyst-layer (R_{CL}) resistances are plotted in Fig.7a as a function of catalyst loading for three cell voltages. The minimum in R_s at 0.17 mg·cm^{-2} is concomitant with the general optimization of cell parameters, ie. the minimum in R_i^{dc} (Fig. 6b) and the maximum A_{Pt} (Figs. 6b), and cell response in Fig. 5. In this case it shows that the ionic conduction in the cell is optimal at this loading. Fig. 7a shows also a minimum in R_{CL} at the same Pt loading, more pronounced at high cell potential (low overpotentials) when the cathode catalyst-layer properties govern the cell response. Such minimum reflects the optimization of the electrochemical kinetics and mass transport in the cathodic catalyst layer.

The analysis of the constant-phase-element parameters in Fig.7b provides some more useful information about the behavior of the electrosprayed catalyst layers. Parameter *n* of this circuit element reflects the dispersion of time constants frequently encountered in solid electrodes, with n=1 for the case of a single time constant, and decreasing ($0<n<1$) by increasing dispersion [42]. For a catalyst layer, dispersion may be larger by increasing the layer thickness because of larger heterogeneities in all parameters affecting its response, e.g., temperature, pressure, potential, current, concentration of reactants, water, etc. Consequently, results in Fig. 7b show that *n* decreases with catalyst loading (film thickness). On the other hand, Y_{CL} shows a continuous increase with the platinum loading, with increasing slope by decreasing cell voltage (increasing the current). The information of interest from this parameter resides in its pseudo-capacitive character which is related with charge storage in the catalyst layer. A capacitance can be determined from Y_{CL} using the following relationship [42,43]:

$$C_{CL} = Y_{CL}^{1/n} R_{CL}^{\left(\frac{1}{n}-1\right)} \qquad (9)$$

Where C_{CL} is the electrical capacitance of the cathodic catalyst layer. The result of the conversion is plotted in Fig.8. A capacitance peak with loading is found at 0.17 mg_{Pt}·cm^{-2} (0.68 mg_C·cm^{-2}), which

shows similar dependence as the electrochemical active platinum area in Fig.6a, although C_{CL} must be related with the whole electrochemical active area of the catalyst layer, ie. C and Pt surfaces (in fact Pt surface has minor contribution compared with carbon black). Fig, 7c includes the nominal capacitance expected for the carbon black surface, taking specific area 210 $m^2 \cdot g_C^{-1}$ and specific capacitance 16 $\mu F \cdot cm^{-2}$ [44], that shows good agreement with the experimental curves only at low loadings. The saturation of the charge storage, together with that observed for the electrocatalyst surface (Fig.6a), indicate that above 0.17 $mg_{Pt} \cdot cm^{-2}$ the additional electrosprayed catalyst layer is electrochemically inactive. Such result may be a consequence of the water transport and wetting properties of superhydrophobic catalyst layers, as explained in the following section.

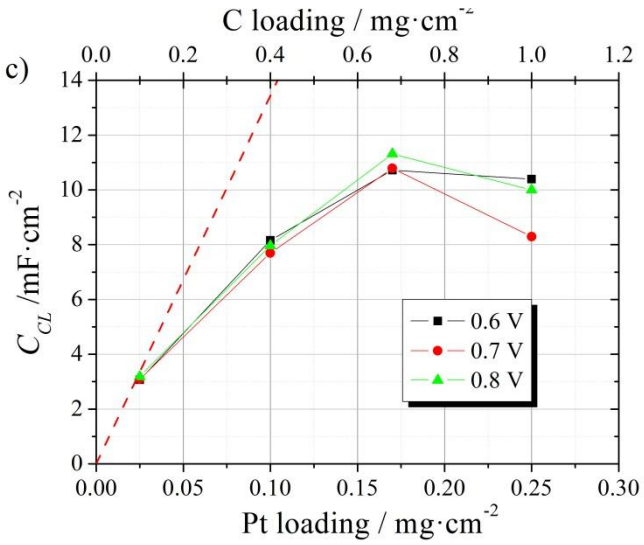

Fig.8. Result of the application of Eq.9 to impedance analysis in Fig. 7b. Dashed red line indicates the estimated nominal capacitance of the carbon black phase.

4. Discussion

Mass transport in electrosprayed catalyst layers is characterized by lower R_{CL}^{mt} values compared with conventional airbrushed layers, up to 25% lower depending on composition and testing conditions. The differences are more important in layers with low platinum loading (Fig. 1b) and at low temperatures (Fig.1d). It is also significant that a low impact on transport resistance is witnessed with ionomer concentration (Fig.1a), which appears to interact preferentially with the Pt phase in the elemental mappings of Pt and F (Fig. 4). Water-vapor uptake capability of electrosprayed catalyst layers is higher than conventional layers (Fig.2, and see also Fig.S2 in Supplementary Material). This reflects that the nanostructure and distribution resulting from the electrosprayed deposition, including the enhanced interaction with Pt, which itself has an important effect on water-vapor uptake, result in an ionomer that more readily absorbs water, and thus exhibits better transport properties. This characteristic is in stark contrast with the superhydrophobicity of electrospray catalyst layers, which show very high liquid water contact angles, above 150^{o}, and low wettability [11,16,17]. Both properties must be a result of a macroporous catalyst layer with highly available hydrophilic groups (sulfonic groups of the ionomer) inside a pore structure which walls, having dendrite growths of the catalyst particles and the ionomer, favor air trapped pockets and preclude liquid-water interaction, like in a Cassie state surface [45]. The combined high water-vapor absorption with superhydrophobicity optimizes the function of a PEMFC catalyst layer under different operation conditions since it provides good ionic conductivity along with superior liquid-water transport characteristics.

The expected enhancement from the ex-situ analysis is observed in single cell testing, where an optimal electrosprayed loading occurs at 0.17 mg·cm^{-2} (using catalyst Pt/C 20wt%) in accordance with that found in previous studies [36], and which corresponds with a layer thickness of 18 µm

(see Supplementary Material, Fig.S4). At this loading, the highest active areas are measured for the Pt surface catalyst and for the carbon surface (Figs.6a and 8, respectively), the second one inferred from larger double-layer capacitance. Also, at this loading, all ohmic resistances (electronic and ionic) are minimized (Fig. 6b).

The experimental mass transport (R_{CL}^{mt}) is a contribution to the catalyst layer resistance (R_{CL}). A simplified picture can be used that considers the second one as composed of three serial contributions:

$$R_{CL} = R_{CL}^{kin} + R_{CL}^{ohm} + f \cdot R_{CL}^{mt} \quad (10)$$

Where R_{CL}^{kin} is the kinetic resistance (charge transfer), and R_{CL}^{ohm} is the ohmic resistance due to protonic and electronic conduction in the catalyst layer ($R_{CL}^{ohm} = R_{CL}^{ohm,H+} + R_{CL}^{ohm,e-}$); f (V cm^3 C^{-1}) is a proportionality factor that takes into account oxygen parameters (molecular weight, n, and concentration) and the change of units. Eq. 10 helps to rationalize the results of mass transport and impedance. The increase in R_{CL} at low loading can be attributed to R_{CL}^{mt}, ie. the local mass transport resistance, and also R_{CL}^{kin} contributes due to the low loading. Other characteristics of the impedance results require considering additional effects. The increase in R_s at low loadings (Fig.7a), which must be related with R_{CL}^{ohm} in Eq.10, reflects a decrease in the electronic or ionic conduction of the catalyst layer; in addition, the slight increase in R_{CL} at high loadings (Fig.7a) cannot be a mass transport effect because R_{CL}^{mt} decreases in the loading range studied here (Fig. 1b).

One possible explanation for the above observations requires considering wetting properties of the catalyst layer as thin porous layer. Below a certain thickness value, electrosprayed film electrodes show electrochemical response very dependent on thickness, as observed for carbon black films which electrochemical active area shows peaks at 40 µm (0.2 mg$_C$·cm^{-2}) [34]. Such

behavior can only be explained as a consequence of particular wetting properties of the superhydrophobic 'thin porous film' having a thickness lower or comparable with their characteristic pores size. It is known that thin porous films have different properties than thicker ones, like permeability, wetting, and water transport [46]. On this ground, an explanation can be proposed for the trends observed in the impedance response and mass transport of the electrosprayed catalyst layers (cf. Fig S7 in Supplementary Material). At very low thickness, the thin porous layer in contact with the fully humidified PEM is flooded because no capillary pressure is developed to repeal the liquid water of the PEM, so water invasion occurs. Therefore, very thin catalyst-layers are characterised by high R_{CL}^{mt} ('through plane' resistances term in Eq.1) and $R_{CL}^{ohm,e-}$ (electronic resistance component due to loss of inter-particles contact in a flooded layer). Increasing catalyst-layer thickness makes possible capillary forces to decrease liquid water saturation and a decrease in R_{CL}^{mt} and R_{CL}^{ohm} is observed (Figs.1b and 7a), up to a certain thickness where the superhydrophobic catalyst layer impose too dry conditions which increases the protonic resistance ($R_{CL}^{ohm,H+}$) and decreases catalyst utilization (Fig.6a). There is, therefore, an optimal thickness that allows for mixed wettability and partially saturated layer, leading to the lowest mass transport, electronic, and protonic resistances, and maximum Pt utilization. For the case of electrosprayed films with Pt/C 20wt% the thickness is 18 µm (0.17 $mg_{Pt}{\cdot}cm^{-2}$). Decreasing the optimal catalyst loading, therefore, requires maintaining the optimal thickness in order to avoid flooding in too thin layers. In the Supplementary Material, Fig.S7, a scheme depicts schematically the three characteristics saturation states for a superhydrophobic catalyst layer in dependence of thickness.

5. Conclusions

Transport properties of catalyst layers prepared by electrospray deposition have been studied by mass-transport-resistance measurements and correlated with water-vapor uptake, ionomer phase distribution imaging, and single-cell performance. The following conclusions have been obtained from the study:

- Low mass transport resistance reveals improved transport properties of electrosprayed catalyst layers compared with conventional layers.

- Water-vapor uptake is larger for electrosprayed layer that we attribute to the particular morphology and distribution of the ionomer phase, which shows a specific interaction with the platinum surface.

- The enhanced water-vapor uptake of electrosprayed layers combined with their very low wettability and superhydrophobic character, studied in previous works, allow for an optimal catalyst layer with low mass transport resistance and high ionic conductivity.

- Single cell results reveal an optimal Pt loading of 0.17 $mgPt \cdot cm^{-2}$ for electrosprayed layers prepared with Pt/C 20wt% catalyst, that correspond to the thickness of 18 μm. Such layer allows for optimal mass transport, catalyst utilization, and ionic conductivity. Decreasing the optimal loading requires keeping similar catalyst layer thickness to avoid local mass transport losses and flooding that occurs in too thin layers.

Acknowledgements

This work was supported by the Ministerio de Economía y Competitividad of Spain, and Fondo Europeo de Desarrollo Regional (FEDER), Project E-LIG-E, ENE2015-70417-P (MINECO/FEDER).

Microscopy conducted at ORNL's Center for Nanophase Materials Sciences, which is a U.S. DOE Office of Science User Facility. LBNL and ORNL research was supported by the Fuel Cell Technologies Office, Office of Energy Efficiency and Renewable Energy, U.S. DOE, and was conducted through the FC-PAD Consortium.

References

[1] T.E. Springer, T.A. Zawodzinski, S. Gottesfeld, Polymer Electrolyte Fuel Cell Model, J. Electrochem. Soc. 138 (1991) 2334-2342. https://doi.org/10.1149/1.2085971

[2] A.Z. Weber, J. Newman, Modeling Transport in Polymer-Electrolyte Fuel Cells, Chem. Rev. 104 (2004) 4679-4726.

[3] S. Litster, G. McLean, PEM fuel cell electrodes, J. Power Sources 130 (2004) 61–76.

[4] A.M. Chaparro, R. Benítez, L. Gubler, G.G. Scherer, L. Daza, Study of membrane electrode assemblies for PEMFC with cathodes prepared by the electrospray method, J. Power Sources 169 (2007) 77–84.

[5] A. M. Chaparro, M. A. Folgado, P. Ferreira-Aparicio, A. J. Martín, I. Alonso-Álvarez, L. Daza, Properties of Catalyst Layers for PEMFC Electrodes Prepared by Electrospray Deposition, J. Electrochem. Soc. 157 (2010) B993-B999.

[6] S. Martin, P. L. Garcia-Ybarra, J. L. Castillo, High platinum utilization in ultra-low Pt loaded PEM fuel cell cathodes prepared by electrospraying, Int. J. Hydrogen Ener. 35 (2010) 10446-10451.

[7] K. Takahashi, K. Kakinuma, M. Uchida, Improvement of Cell Performance in Low-Pt-Loading PEFC Cathode Catalyst Layers Prepared by the Electrospray Method, J. Electrochem. Soc. 163 (2016) F1182-F1188.

[8] B-S. Koh, J-H. Yoo, E-K Jang, V. R. Jothi, C-Y. Jung, S.C. Yi, Fabrication of highly effective self-humidifying membrane electrode assembly for proton exchange membrane fuel cells via electrostatic spray deposition, Electrochem. Comm. 93 (2018) 76–80.

[9] N. Chingthamai, K. Sombatmankhong, Y. Laoonual, Experimental investigation of electrospray coating technique for electrode fabrication in PEMFCs, Energy Procedia 105 (2017) 1806 – 1812.

[10] A.M. Chaparro, P. Ferreira-Aparicio, M.A. Folgado, A.J. Martín, L. Daza, Catalyst layers for proton exchange membrane fuel cells prepared by electrospray deposition on Nafion membrane, J. Power Sources 196 (2011) 4200–4208.

[11] A.M. Chaparro, P. Ferreira-Aparicio, M.A. Folgado, E. Brightman, G. Hinds, Study of superhydrophobic electrosprayed catalyst layers using a localized reference electrode technique, J. Power Sources 325 (2016) 609-619.

[12] J. Bear, Dynamics of Fluids in Porous Media, Dover Publications, Inc., New York, 1988.

[13] T. Hutzenlaub, J. Becker, R. Zengerle, S. Thiele, Modelling the water distribution within a hydrophilic and hydrophobic 3D reconstructed cathode catalyst layer of a proton exchange membrane fuel cell, J. Power Sources 227 (2013) 260-266.

[14] X. Wang, T. Van Nguyen, Modeling the Effects of Capillary Property of Porous Media on the Performance of the Cathode of a PEMFC, J. Electrochem. Soc. 155 (2008) B1085-B1092.

[15] M. El Hannach, M. Prat, J. Pauchet, Pore network model of the cathode catalyst layer of proton exchange membrane fuel cells: Analysis of water management and electrical performance, Int. J. Hydrogen Ener. 37 (2012) 18996-19006.

[16] P. Ferreira-Aparicio, A.M. Chaparro, M. A. Folgado, J.J. Conde, E. Brightman, G. Hinds, Degradation Study by Start-Up/Shut-Down Cycling of Superhydrophobic Electrosprayed Catalyst Layers Using a Localized Reference Electrode Technique, ACS Appl. Mater. Interf. 9 (2017) 10626−10636.

[17] M.A. Folgado, J.J. Conde, P. Ferreira-Aparicio, A.M. Chaparro, Single Cell Study of Water Transport in PEMFCs with Electrosprayed Catalyst Layers, Fuel Cells 18 (2018) 602-612. https://doi.org/10.1002/fuce.201700217

[18] T.A. Greszler, D. Caulk, P. Sinha, The Impact of Platinum Loading on Oxygen Transport Resistance, J. Electrochem. Soc. 159 (2012) F831-F840.

[19] G.S. Hwang, A.Z. Weber, Effective-Diffusivity Measurement of Partially-Saturated Fuel-Cell Gas-Diffusion Layers, J. Electrochem. Soc. 159 (2012) F683-F692.

[20] A.Z. Weber, A. Kusoglu, Unexplained transport resistances for low-loaded fuel-cell catalyst layers. J Mater. Chem. A. 2 (2014) 17207-17211.

[21] A. Kongkanand, M.F. Mathias, The Priority and Challenge of High-Power Performance of Low-Platinum Proton-Exchange Membrane Fuel Cells, J. Phys. Chem. Letters 7 (2016) 1127-1137.

[22] F.B. Spingler, A. Phillips, T. Schuler, M.C. Tucker, A.Z. Weber, Investigating Fuel-Cell Transport Limitations using Hydrogen Limiting Current, Int. J. Hydrogen Ener. 42 (2017) 13960-13969.

[23] N. Nonoyama, S. Okazaki, A.Z. Weber, Y. Ikogi, T. Yoshida, Analysis of Oxygen-Transport Diffusion Resistance in Proton-Exchange-Membrane Fuel Cells, J. Electrochem. Soc. 158 (2011) B416-B423. https://doi.org/10.1149/1.3546038

[24] J.P. Owejan, J.E. Owejan, W. Gu, Impact of platinum loading and catalyst layer structure on PEMFC performance, J. Electrochem. Soc. 160 (2013) F824-F833.

[25] D.R. Baker, D.A. Caulk, K.C. Neyerlin, M.W. Murphy, Measurement of Oxygen Transport Resistance in PEM Fuel Cells by Limiting Current Methods, J. Electrochem. Soc. 156 (2009) B991-B1003.

[26] Y. Ono, T. Mashio, S. Takaichi, A. Ohma, H. Kanesaka, K. Shinohara, The analysis of performance loss with low platinum loaded cathode catalyst layer, ECS Transaction 28 (27) (2010) 69-78.

[27] A.T.S. Freiberg, M.C. Tucker, A.Z. Weber, Polarization Loss Correction Derived from Hydrogen Local-Resistance Measurement in Low Pt-Loaded Polymer-Electrolyte Fuel Cells, Electrochem. Comm. 79 (2017) 14-17.

[28] T. Schuler, A. Chowdhury, A.T. Freiberg, B. Sneed, F.B. Spingler, M.C. Tucker, K.L. More, C.J. Radke, A.Z. Weber, Fuel-cell Catalyst-Layer resistance Via Hydrogen Limiting-Current Measurements, J. Electrochem. Soc. 166(7) (2019) F3020-F3031.

[29] A. Chowdhury, C. J. Radke, A. Z. Weber, Transport Resistances in Fuel-Cell Catalyst Layers, ECS Transaction 80 (8) (2017) 321-333. https://doi.org/10.1149/08008.0321ecst

[30] R. Koestner, D.Cullen, R. Kukreja, S. Minko, H.M. Meyer, Z.Liu and K.L. More , High-Resolution Mapping of the PFSA Polymer Distribution in PEFC Electrode Layers, ECS Trans. 64 (3) (2014) 819-827.

[31] D. A. Cullen, R. Koestner, R. S. Kukrej, Z. Y. Liu, S. Minko, O. Trotsenko, A. Tokarev, L. Guetaz, H. M. Meyer III, C. M. Parish, and K. L. Moref, Imaging and Microanalysis of Thin Ionomer Layers by Scanning Transmission Electron Microscopy, J. Electrochem. Soc. 161 (10) (2014) F1111-F1117.

[32] A. Kusoglu, A. Kwong, K.T. Clark, H.P. Gunterman, A.Z. Weber, Water Uptake of Fuel-Cell Catalyst Layers, J. Electrochem. Soc. 159 (9) (2012) F530-F535.

[33] J.J. Conde, A.M. Chaparro, P. Ferreira-Aparicio, Understanding the Behavior of Electrosprayed Carbon Black-Nafion Composite Layers, Fuel Cells 18 (2018) 627-639. https://doi.org/10.1002/fuce.201700218.

[34] J.J. Conde, P. Ferreira-Aparicio, A.M. Chaparro, Anti-corrosion coating for metal surfaces based on superhydrophobic electrosprayed carbon layers, App. Mat. Today 13 (2018) 100–106.

[35] Y.-C. Park, H. Tokiwa, K. Kakinuma, M. Watanabe, M. Uchida, Effects of carbon supports on Pt distribution, ionomer coverage and cathode performance for polymer electrolyte fuel cells, J. Power Sources 315 (2016) 179-191.

[36] A.M. Chaparro, B. Gallardo, M.A. Folgado, A.J. Martín, L. Daza, PEMFC electrode preparation by electrospray: Optimization of catalyst load and ionomer content, Catalysis Today 143 (2009) 237–241.

[37] K. C. Neyerlin, W. Gu, J. Jorne, H. A. Gasteiger, Determination of Catalyst Unique Parameters for the Oxygen Reduction Reaction in a PEMFC, J. Electrochem. Soc. 153 (2006) A1955-A1963. https://doi.org/10.1149/1.2266294.

[38] M. Lee, M. Uchida, D.A. Tryk, H. Uchida, M. Watanabe, The effectiveness of platinum/carbon electrocatalysts: Dependence on catalyst layer thickness and Pt alloy catalytic effects, Electrochim. Acta, 56 (2011) 4783-4790.

[39] T. Suzuki, S. Tsushima, S. Hirai, Fabrication and performance evaluation of structurally-controlled PEMFC catalyst layers by blending platinum-supported and stand-alone carbon black, J. Power Sources 233 (2013) 269-276.

[40] F.A. Uribe, T.E. Springer, S. Gottesfeld, A microelectrode study of oxygen reduction at the platinum/recast-Nafion film interface, J. Electrochem. Soc. 139 (1992) 765-773.

[41] E. Springer, A. Zawodzinski, M. S. Wilson, S. Gottesfeld, Characterization of Polymer Electrolyte Fuel Cells Using AC Impedance Spectroscopy, J. Electrochem. Soc. 143(2) (1996) 587-599.

[42] A. Lasia, Impedance of porous electrodes, J. Electroanal. Chem. 397 (1995) 27-33.

[43] W.G. Pell, A. Zolfaghari, B. E. Conway, Capacitance of the double-layer at polycrystalline Pt electrodes bearing a surface-oxide film, J. Electroanal. Chem. 532 (2002) 13-23.

[44] F. Beck, M. Dolata, E. Grivei, N. Probst, Electrochemical supercapacitors based on industrial carbon blacks in aqueous H2SO4, J. Appl. Electrochem. 31 (2001) 845-853.

[45] D. Quéré, Wetting and Roughness, Annu. Rev. Mater. Res. 38 (2008) 71–99.

[46] M. Prat, T. Agaësse, Thin Porous Media, in: Kambiz Vafai (Ed.), Handbook of Porous Media, 3rd Edition, CRC Press, Boca Raton, 2015, pp. 89-112.